Corrosion Science 123 (2017) 297–309

Contents lists available at ScienceDirect

Corrosion Science

journal homepage: www.elsevier.com/locate/corsci

# Understanding the effect of magnesium degradation on drug release and anti-proliferation on smooth muscle cells for magnesium-based drug eluting stents

Yongjuan Shi[a], Jia Pei[a,*], Lei Zhang[a], Byung Kook Lee[b], Yeonhee Yun[b], Jian Zhang[a], Zhonghua Li[c], Song Gu[d], Kinam Park[b], Guangyin Yuan[a,*]

[a] National Engineering Research Center of Light Alloy Net Forming & State Key Laboratory of Metal Matrix Composite, Shanghai Jiao Tong University, Shanghai, 200240, China
[b] Weldon School of Biomedical Engineering, Purdue University, IN, 47907, United States
[c] Microport Endovascular (Shanghai) Co., Ltd, Shanghai, 201318, China
[d] Shanghai Children's Medical Center, Shanghai Jiao Tong University, Shanghai, 200127, China

ARTICLE INFO

*Keywords:*
A. Magnesium
A. Organic coatings
A. Polymer
B. Erosion
C. Interfaces
C. Kinetic parameters

ABSTRACT

To understand the possible influence of substrate degradation on the drug-loading system of magnesium alloy-based drug-eluting stents, a rapamycin drug-loading poly(lactic-co-glycolic acid) coating was prepared on Mg-Nd-Zn-Zr stents for a systematic investigation in a phosphate buffer system. Mg degradation accelerated the drug release kinetics prominently, which was mainly attributed to $H_2$ evolution in the diffusion-controlled phase while thereafter to PLGA erosion. Although physiochemical stability of the released rapamycin was partially deteriorated by magnesium degradation, the drug-loading system on magnesium substrates exhibited a more potent long-term inhibition on smooth muscle cell proliferation in vitro as compared to drug-loaded stainless steel.

## 1. Introduction

In the last decade, implantation of drug-eluting stents (DESs) has revolutionized the interventional cardiology in treating diseased coronary arteries. Benefiting from the local release of the loaded drugs, the risk of restenosis following stenting has been shown to be further reduced or even eliminated compared with bare metal stents [1–3]. Conventional stent materials including stainless steel, nickel-titanium alloy and tantalum, generally passive metal based, however, have posed clinical limitations which are most possibly associated with the permanent presence of artificial implants [4–7]. Attempt has been recently fostered to deploy absorbable stents composed of biodegradable materials for temporary structural support until the recovery of arteries, accompanied with complete degradation/absorption of implant materials over time.

Among various biodegradable materials, magnesium alloys have attracted intense interest thanks to their desirable mechanical properties and great biosafety [8]. A number of studies [9–16] focused on the promising use of Mg alloys as temporary cardiovascular stents, and DESs have emerged since the first successful implantation of a Mg stent into the left pulmonary artery of a preterm baby [17]. Recently developed magnesium alloy-based drug-eluting stents DREAMS and DREAMS 2G, offering antiproliferative drug (paclitaxel or rapamycin) elution as well as a slower stent degradation compared with the bare Mg stent, were successively tested in the BIOSOLVE-I and BIOSOLVE-II clinical trials, exhibiting favorable biosafety and efficacy with no death and no obvious scaffold thrombosis [10,15,18].

For DES application, local drug release kinetics and releasing mechanisms are crucial in inhibiting vascular smooth muscle cell (SMC) proliferation, neointimal hyperplasia and lumen renarrowing, consequently determining the clinical efficacy of DES treatment, e.g. rates of restenosis and neointimal proliferation [19]. Though biodegradable Mg-based DES has revealed great prospect for wide clinical use to substitute the conventional passive, there is still a lack of fundamental understanding of the interactions between magnesium substrate and drug loading system with regard to drug eluting process, by which the performance of DESs would be largely affected. As in contrast to passive stent materials, Mg-based substrate is easy to be subjected to corrosion/degradation in aqueous media, according to the Eq. (1) [20].

$$Mg(s) + 2H_2O(aq) \rightleftharpoons Mg(OH)_2(s) + H_2(g)\uparrow \quad (1)$$

* Corresponding authors.
*E-mail addresses:* jpei@sjtu.edu.cn (J. Pei), gyyuan@sjtu.edu.cn (G. Yuan).

http://dx.doi.org/10.1016/j.corsci.2017.04.016
Received 20 December 2016; Received in revised form 21 April 2017; Accepted 22 April 2017
Available online 04 May 2017
0010-938X/ 

Insoluble $Mg(OH)_2$ is formed once the metal reaches direct contact with water, but it is not stable in the presence of anions like $Cl^-$, $SO_4^{2-}$ or under acidic conditions [21,22]:

$$Mg(OH)_2(s) \rightleftharpoons Mg^{2+}(aq) + 2OH^-(aq) \quad (2)$$

Thus, the degradation of Mg substrate inevitably leads to environmental changes in $Mg^{2+}$ concentration, pH, hydrogen evolution and other physiochemical conditions [8,23]. While a lot of efforts were recently made to investigate the influence of the released $Mg^{2+}$ on vascular-related cellular responses [24], the impact of other changes, such as hydrogen evolution and pH increase that are likely to exert on the loaded drug elution and the subsequent effect on cells, has been rarely studied and remains unclear so far.

Generally, modern DESs are comprised of three parts − a stent platform, a coating, typically polymeric, that loads and elutes drugs, and the drug, mainly immunosuppressive and antiproliferative agents to inhibit neointimal hyperplasia. Regarding stent platform, one of the most challenging problems for application of Mg alloys lies in the high degradation rate as well as the localized corrosion [25,26], which could result in early fractures and failure of stents due to the lack of sufficient supporting strength. Previously in our group, a novel Mg-Nd-Zn-Zr alloy (named JDBM) has been developed owning nanophasic uniform degradation characteristic [27] and low corrosion rate [28]. Surface treatment generating a thin $MgF_2$ conversion layer further enhanced its durability and biocompatibility [21,29], thus presenting as a promising candidate for DES platform. Poly(lactic-co-glycolic acid) (PLGA) is a type of physically strong, biocompatible and biodegradable polymer [30]. It has been extensively applied as drug delivery vehicles, scaffolds for tissue engineering, and drug-loaded coatings for stents and other implants as well [31–33]. Rapamycin (RAPA), which inhibits in-stent restenosis by binding and prohibiting the mammalian target of rapamycin (mTOR), arresting the G1-S phase in the cell cycle [34] and therefore inhibiting the proliferation of smooth muscle cells, are intensively used as an anti-restenosis agent in DESs for its superior anti-proliferation and immunosuppressant properties [35].

Here, a drug eluting system composed of PLGA coatings as drug carrier loaded with RAPA were prepared on JDBM substrates with a protective $MgF_2$ conversion coating, in order to conduct a systematic study of the potential effect of Mg degradation on the in vitro RAPA release profiles, drug stability as well as the underlying release mechanisms in a phosphate buffer system. The resultant anti-proliferative effectiveness was quantitatively evaluated with smooth muscle-derived cell line. As one of the conventional passive stent materials, stainless steel corrodes so slow that once it is implanted into body it is most likely to stay life-long time, therefore, 316 L stainless steel (hereafter denoted as 316 L SS) drug-eluting system served as the control group of passive substrate throughout the study.

## 2. Materials and methods

### 2.1. Materials

Mg-Nd-Zn-Zr alloy (detailed composition listed in Table 1a) was used as the substrate material, and the specimens were prepared in the same way as in ref. [21]. Commercial 316 L SS (detailed composition listed in Table 1b), was employed as the control substrate group. PLGA (mole ratio of LA/GA = 75/25) with a weight-average molecular weight of ~100,000 g/mol was supplied by Akina, Inc., USA. Rapamycin (RAPA, > 99%) was purchased from Shanghai Baibo Biotechnology Co., Ltd. (Shanghai, China). Hydrofluoric acid (40 wt.%) of analytical grade, methanol, acetonitrile and ethyl acetate of HPLC grade were obtained from Sinopharm Chemical Reagent Co., Ltd. (Shanghai, China).

**Table 1a**
The chemical composition of Mg-Nd-Zn-Zr alloy.

| Element | Mg | Nd | Zn | Zr | Mn | Si | Cu | Fe |
|---|---|---|---|---|---|---|---|---|
| wt.% | balance | 2.1 | 0.21 | 0.5 | 0.009 | 0.006 | 0.005 | 0.002 |

### 2.2. Sample preparation

Since the corrosion resistance of bare magnesium alloy is poor for clinical application, in this paper, all the Mg-alloy based stents and disks were pre-treated in hydrofluoric acid for 14 h to form a protective $MgF_2$ layer of ~1.5 μm thickness to retard the rapid corrosion of the bare Mg-Nd-Zn-Zr alloy (denoted F-JDBM) [21].

F-JDBM and 316 L SS stents of an identical structure were fabricated by a laser cutting technology. A hybrid solution containing PLGA and RAPA with an overall solid concentration of 1 w/v% was prepared and the ratio of RAPA/PLGA was 12 wt.%. F-JDBM and 316 L SS-based DESs were prepared using a rotary ultrasonic spray-coating technology as described in ref [36] to obtain a drug loading of 1.4 ± 0.2 μg/mm$^2$.

JDBM and 316 L SS disk specimens (ϕ15 × 3 mm) were ground with SiC paper up to 3000 grit, cleaned in acetone and ethanol, respectively, dried with warm air and followed by the treatment with hydrofluoric acid. Coatings (PLGA or PLGA/RAPA coating) were prepared by a solvent casting method. Precisely, 100 μL of the pre-prepared solution with a total polymer and drug concentration of 2 w/v % was dropped on top surfaces of F-JDBM and 316L SS disks followed by drying for 24 h in a chemical hood to obtain similar coating thickness as the DESs. All the coated stents and disk samples were subsequently transferred to a vacuum chamber for further drying for at least 48 h.

For simplicity, acronyms for the samples with different coatings are listed in Table 2.

### 2.3. Physicochemical characterizations

The surfaces of the drug-eluting stents (DESs) were observed using a scanning electronic microscope (SEM, FEI NOVA NANOSEM 200, USA) after coated with a thin layer of silver by a sputter coater (Cresington 208 HR, USA). Fourier transform infrared spectroscopy (FTIR, Nicolet 6700, ThermoFisher, USA) was used to examine the chemical structure of PLGA, RAPA and PLGA/RAPA coatings on disk samples in the wave number range of 4000–600 cm$^{-1}$. The X-ray diffraction (XRD) patterns of PLGA film, PLGA/RAPA film, and pure RAPA were characterized using X-ray diffractometer (Smart Lab, Japan) and data in the angular region of 2θ = 5–40° were collected at room temperature.

### 2.4. In vitro RAPA release

F-JDBM and 316L SS DESs were immersed into 3 mL of phosphate buffer saline (PBS, NaCl 8.0 g/L, KCl 0.2 g/L, $Na_2HPO_4$ 1.44 g/L,$KH_2PO_4$ 0.24 g/L) containing 0.5 v/v% Tween 20 (denoted as PBST), respectively. A slight amount of Tween 20 was added to increase the solubility of RAPA in PBS. After placed in a shaking incubator (80 rpm, 37 °C) for predetermined time intervals, the releasing medium was collected and replaced with fresh PBST. Subsequently the filtrate through 0.2 μm filters (Millex GPfilter unit, Millipore, USA) was collected, and the RAPA concentration in the release medium was measured using a bio UV/Vis spectrophotometer (Thermo Spectronic Genesys 10, USA) at the wavelength of 278 nm. The pH of the release medium was monitored with a pH meter (VWR SympHony SB70P, USA). In addition, at the end of the entire test of 60 days, the surface morphologies of the specimens were observed using SEM.

### 2.5. $H_2$ evolution

The hydrogen evolution test was carried out as depicted in Ref. [37]. The disk samples were suspended in beakers containing c-SBF

**Table 1b**
The chemical composition of 316 L stainless steel.

| Element | Fe | Cr | Ni | Mo | Mn | Cu | Si | C | N | S | P |
|---|---|---|---|---|---|---|---|---|---|---|---|
| wt.% | balance | 17.5 | 13.07 | 2.66 | 1.06 | 0.05 | 0.6 | 0.025 | 0.004 | 0.008 | 0.002 |

**Table 2**
List of the acronyms used in this paper.

| Sample Description | Acronym |
|---|---|
| Bare Mg-Nd-Zn-Zr | JDBM |
| HF-pretreated Mg-Nd-Zn-Zr | F-JDBM |
| PLGA-coated Mg-Nd-Zn-Zr pretreated with HF | PF-JDBM |
| PLGA/RAPA-coated Mg-Nd-Zn-Zr pretreated with HF | PRF-JDBM |
| PLGA/RAPA-coated 316 L stainless steel | PR-316 L SS |
| Drug-eluting stents | DESs |
| Rapamycin | RAPA |
| Poly(lactic-co-glycolic acid) | PLGA |
| Lactic acid/glycolic acid | LA/GA |

(NaCl 8.036 g/L, $NaCO_3$ 0.352 g/L, KCl 0.225 g/L, $K_2HPO_3{\cdot}3H_2O$ 0.230 g/L, $MgCl_2{\cdot}6H_2O$ 0.311 g/L, 1.0 M HCl 40 mL/L, $CaCl_2$ 0.293 g/L, $Na_2SO_4$ 0.072 g/L, Tris 6.063 g/L, buffered with 1.0 M HCl to pH 7.4 at 37 °C) with a funnel placed over the specimens to collect the hydrogen evolved from the specimen. A burette was mounted over the funnel and filled with solution. In this way, the volume of the evolved hydrogen was measured.

### 2.6. Factors affecting the drug release from F-JDBM DESs

During the drug release process of F-JDBM DESs, due to the degradation of Mg alloy, the release system was expected to experience obvious changes in two aspects: the increase of pH, and the $H_2$ evolution. In order to investigate the respective influence of pH change and $H_2$ release on the drug release, two sets of experiments were designed as follows (shown in Fig. 1).

#### 2.6.1. The effect of pH

The effect of pH of the media on the drug release kinetics was examined by monitoring drug release profiles from PLGA/RAPA coatings on 316 L SS disk samples in 5 mL of PBST of pH 7.4 (Group a1), 8.4 (Group a2) and 9.7 (Group a3), respectively, as illustrated in Fig. 1a. At each predetermined time point, the solutions were all replaced with fresh medium in order to keep the pH stable during the entire test process (60 days).

#### 2.6.2. The effect of $H_2$ release

The effect of $H_2$ evolution on drug release profiles was investigated following the experiment shown in Fig. 1b in PBST. Two experimental groups (noted Group b1 and Group b2, respectively) with each group containing a 316 L SS and a F-JDBM sample were designed for comparison. In group b1, the 316 L SS was coated with PLGA/RAPA, and the F-JDBM with bare PLGA; while in group b2, vice versa. In each group, the two samples were placed in a flat-bottomed container and separated by a piece of glass to ensure there was no contact between the samples, which is likely to cause galvanic corrosion. The drug release kinetics measurement was carried out in 10 mL of PBST for a period of 36 days, and the release medium was replaced periodically.

### 2.7. Effect of magnesium degradation on PLGA hydrolysis

The effect of magnesium degradation on PLGA hydrolysis was investigated by immersing PRF-JDBM and PR–316 L SS samples separately in different tubes containing 10 mL of PBST (pH 7.4) for ~2 months. Corresponding to the drug release tests, the medium in each tube was regularly replaced in the same manner as described in sec.2.6. After immersion in PBST for predetermined time, the samples were taken out, rinsed thoroughly with deionized water and dried in a vacuum chamber. The surface morphologies of the hydrolyzed PLGA coating on both F-JDBM and 316 L SS substrates were then observed using SEM.

### 2.8. RAPA stability measurement

As RAPA is not stable in PBS, certain amount of isopropyl alcohol (IPA) is required to increase its stability [38]. In this study, IPA was added to PBS (30% v/v) to minimize the effect of PBS on the stability of RAPA, as well as to improve the solubility of RAPA in aqueous medium.

To study the effect of Mg degradation on the stability of RAPA, a 10 μg/mL RAPA solution was prepared by dissolving RAPA in PBS containing 30% v/v IPA, and then bare JDBM, F-JDBM and SS specimens were immersed in the solution, separately. After incubation for 1 d and 2 d, high performance liquid chromatography (HPLC) results of RAPA were recorded using an HPLC system (Agilent 1100 series, USA) with UV detection at 278 nm. All the tests were run with a flow rate of 1 mL/min at 60 °C through an Agilent C18 column

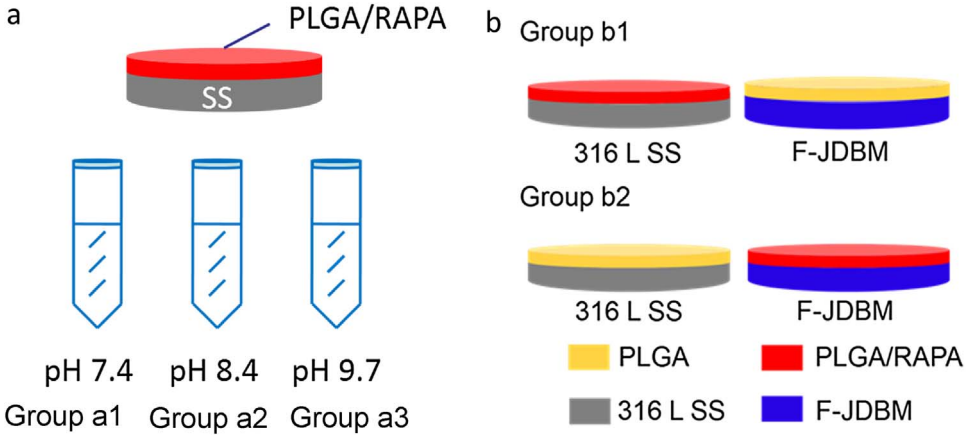


**Fig. 1.** Experimental designs to investigate the respective influence of pH (a) and $H_2$ release (b) on drug release from PLGA/RAPA coatings. The results of experiment (a) and (b) are respectively displayed in Fig. 5(a) and (c).

(5 μm × 4.6 mm × 25 cm). Acetonitrile, methanol and water of HPLC grade in the ratio of 40:40:20 (v/v) was used as a mobile phase and the injection volume was 20 μL.

### 2.9. Cell adhesion and proliferation assays

The rat aorta smooth muscle cell line (A7r5) was purchased from the Cell Bank, Chinese Academy of Sciences. The cells were cultured in Dulbecco's Modified Eagle Medium [39] (DMEM, Gibco, Invitrogen) supplemented with 10% fetal bovine serum (FBS, Gibco, Invitrogen), 100 units/mL penicillin (Gibco, Invitrogen), and 100 units/mL streptomycin (Gibco, Invitrogen) in a cell incubator (humidified atmosphere with 5% $CO_2$ at 37 °C). The cells were used for passages of 4–10 in this study.

Disk samples of PF-JDBM and PRF-JDBM were placed in a 24-well plate with 1 mL of $1 \times 10^4$/mL cell suspension added onto each well. After 24 h and 72 h of incubation, respectively, the samples were gently rinsed with PBS, and stained with calcein acetoxymethyl dye (Calcein-AM, Sigma, US) at a concentration of 0.5 μg/mL for 15 min, followed by gentle washing with PBS. Observation was then conducted with inverted fluorescence microscopy (IX 71, Olympus). Cells in the blank well were used as negative control (NC).

Moreover, in order to evaluate the long-term proliferation inhibition of the drug-loaded F-JDBM and 316 L SS samples, the PRF-JDBM and PR–316 L SS samples were immersed in DMEM for 10 days to eliminate the burst drug release, during which DMEM was replaced every 3 days to avoid reaching drug saturation solubility in the medium. Thereafter cell proliferation assay was conducted on the samples as described above.

### 2.10. Statistics and data analysis

The results were expressed as the mean ± SD. The variance among different groups was analyzed with one-way ANOVA method using SPSS software and statistical significance was set at $p < 0.05$. All the cell experiments were conducted in triplicate for each group at each time, and the assays were repeated at least twice.

## 3. Results

### 3.1. Physiochemical characterizations

Fig. 2a shows the stent structure used to fabricate drug-eluting stents, and the size of the strut is designed to be 160 × 150 μm. SEM images in Fig. 2b and c show smooth outer and inner surface texture of PLGA/RAPA coating on the stent platforms, without any web formation. No drug crystals were observed on the surface, indicating that RAPA was well integrated in the PLGA matrix without phase separation. The thickness of the coating was calculated according to the equation $h = m/\rho S$ (h, m, ρ, S refer to the thickness, the mass, the density and the surface area of the coating, respectively) to be about 4–6 μm.

The chemical structures of the coatings were characterized with FTIR and the spectra of PLGA coating, RAPA drug and RAPA-loaded PLGA coating are respectively shown in Fig. 2d. After RAPA loaded into the PLGA film, the characteristic peaks of RAPA were observed-the intensity of the peaks around 2930 $cm^{-1}$ and 1746 $cm^{-1}$ were significantly strengthened, and a shoulder peak at 1644 $cm^{-1}$ appeared. Additionally, the positions of the characteristics peaks of RAPA did not shift in the RAPA-PLGA coating, compared with the spectra of RAPA alone. These results indicated that the drug coexisted with PLGA in a physically dispersed state rather than chemically bonded, and thus the RAPA drug may well maintain its essential biochemical properties and pharmaceutical functions.

The XRD patterns of PLGA, PLGA/RAPA films and pure RAPA are shown in Fig. 2e. The pattern of the pure drug showed sharp peaks indicating the crystalline nature of RAPA, while PLGA displayed only amorphous halo patterns. After loading RAPA into PLGA film, no diffraction peaks associated with RAPA crystal molecules were observed, which indicates that the RAPA drug appeared in amorphous form or monomolecularly dispersed state in PLGA film.

### 3.2. In vitro release profiles

The in vitro drug release kinetics of F-JDBM and 316 L SS-based DESs within 2 months measured with UV–vis spectrophotometry are shown in Fig. 3a. The in vitro RAPA release profile of the F-JDBM DESs showed three well-defined phases: (I) burst release in the 24 h, and (II) slower drug release from day 2 to day 33, followed by a nearly linear release (III) to day 52, after which a plateau was reached due to the almost complete release of the total drug. In contrast, 316 L SS DESs showed a two-stage drug release kinetics profile: (I) burst release in the first 24 h, and (II) extremely slower drug release until the end of the test. It can be seen that the degradation of Mg substrate enhanced the drug release significantly—F-JDBM DESs exhibited considerably higher release rate than that of 316 L SS DESs, with ~ 80% of the overall amount of drug was released by the end of the test, while only less than 20% was released from 316 L SS DESs.

Meanwhile, the corresponding pH changes of the release media during the drug release process were also monitored, displayed in Fig. 3b. It should be noted that at each time interval, release medium was replaced with fresh buffer of pH 7.4. For F-JDBM DES group, the pH rose dramatically in the first week from 7.4 to about 9.0, followed by a fluctuation between pH 8.5 and pH 9.5 until the end of the test. On the contrary, 316 L SS DES group experienced a slightly decrease in terms of pH, which could be mainly attributed to the slow hydrolysis of PLGA, leading to intermediate degradation products with some acid-base functionality, such as carboxylic groups.

The SEM images of the surface morphologies (Fig. 4a and b) at the end of the drug release test demonstrated that the drug-eluting PLGA coating on F-JDBM stent degraded faster than that on 316 L SS platform. Cross-section of the stent strut (Fig. 4c) revealed uniform and extremely slow degradation of the Mg alloy substrate, as the vast majority of the strut (~140 × 130 μm, encircled by black dotted line) remained intact, with no observation of corrosion pits. The degradation product included two layers, an inner compact one (encircled by blue dotted line) attributable to the transformation of the Mg alloy substrate to corrosion product, and an outer loose one, which was predicted to be stable phosphate crystals resulted from the reaction between the corrosion product and the PBS solution. EDS mapping (Fig. 4d) of a partial region (encircled by red dotted line) showed both of the layers were mainly composed of Mg, O, P and Zr, which could be inferred to be magnesium hydroxide, magnesium phosphate, zirconia and zirconium hydroxide.

### 3.3. Factors affecting the enhanced drug release

The degradation of magnesium alloy in aqueous solutions mainly leads to environmental changes in terms of solution alkalinity and the local release of $H_2$. Therefore, the promoted drug release from PLGA/RAPA coating on Mg-based substrates as compared with the passive 316 L SS substrates is assumed to be affected by these two variables. Herein, in order to determine to what extent these two factors respectively contributed to the improvement of drug release, two sets of experiments were designed as described in sec.2.6, with the results displayed and analyzed in Fig. 5.

### 3.4. pH

Fig. 5a Displays the release profiles of RAPA from PR–316 L SS disks in PBST with pH of 7.4, 8.4 and 9.7, respectively. Specimens at various pH showed similar release kinetics that RAPA was released at a slow

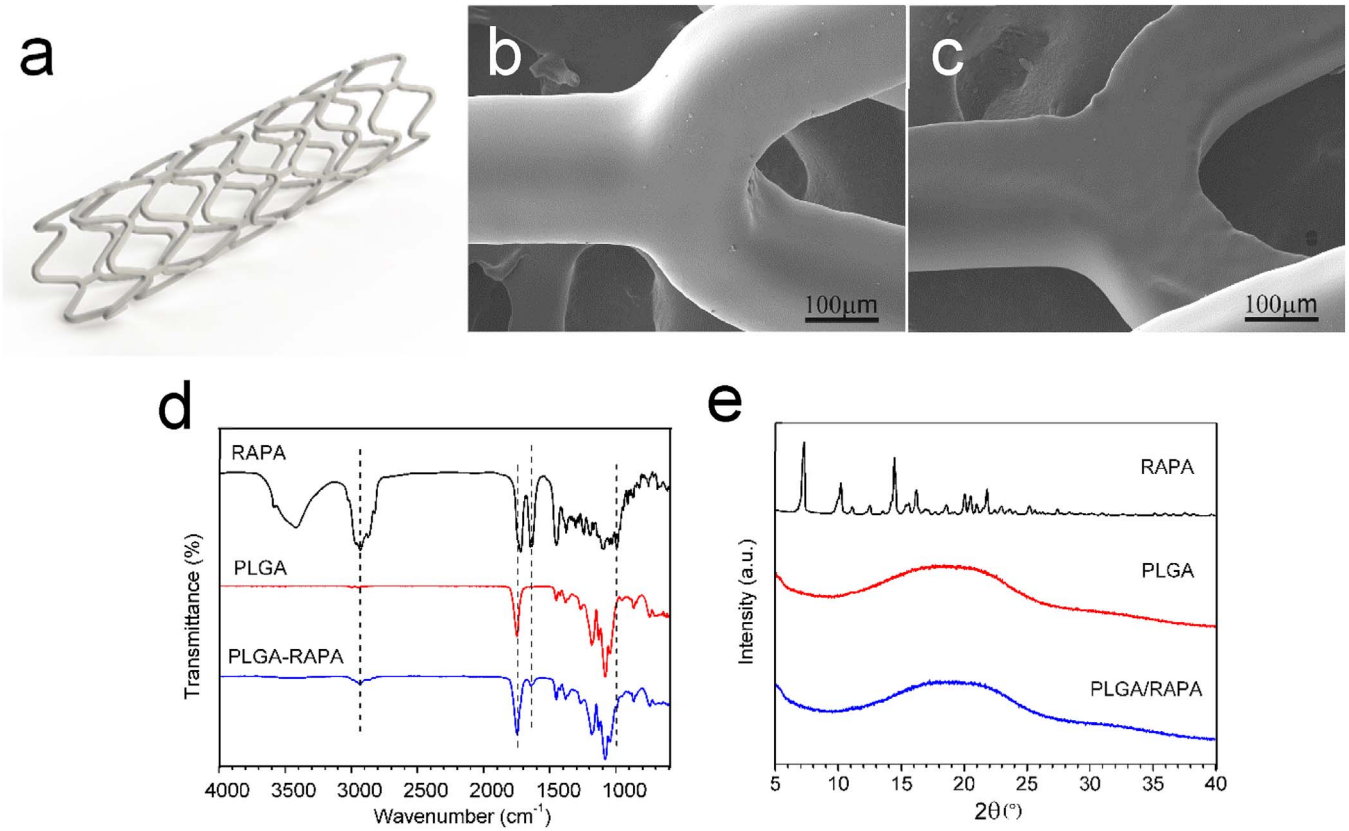


**Fig. 2.** The designed stent structure used in this study (a); SEM images of the outer (b) and inner (c) surface morphologies of F-JDBM DESs; FTIR spectra (d) and XRD patterns (e) of PLGA, RAPA and PLGA/RAPA films.

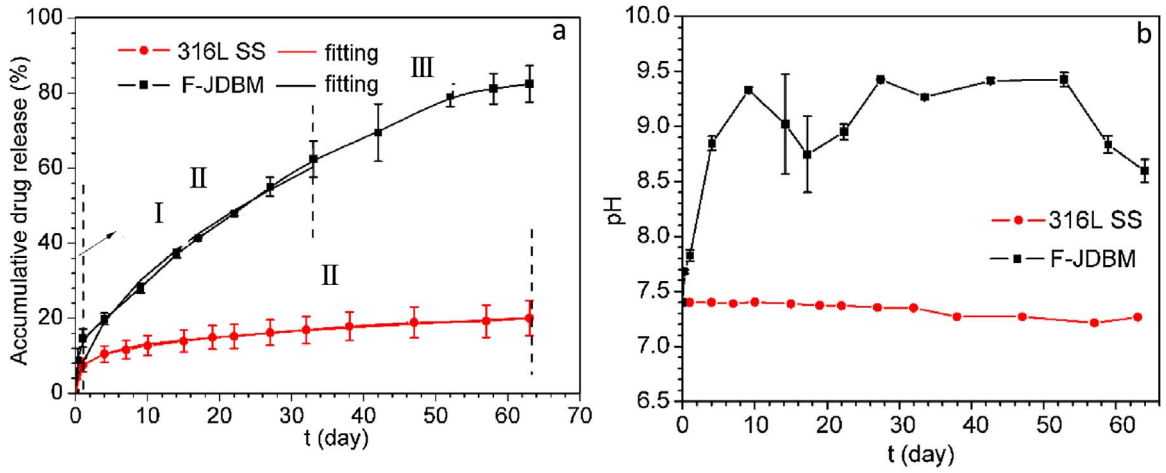


**Fig. 3.** RAPA release profiles for 2 months from PLGA/RAPA coating on F-JDBM and 316 L SS DESs, respectively (a), with curves of phase II are both fitted using Higuchi model; and the pH change of the drug release media during the 2-month period (b).

release rate after the initial burst release at about 22% on the first day, indicating the change of pH in the range of 7.4–9.7 barely affected the release rate.

### 3.5. $H_2$ evolution

$H_2$ evolution profiles of PF-JDBM and PRF-JDBM samples in c-SBF shown in Fig. 6 demonstrated that the addition of 12 wt.% RAPA did not affect the protective effect of PLGA coating. Therefore, the two groups described in sec.2.6b were conceived to show identical degradation rates, leading to analogous pH environments in both containers, which was confirmed by monitoring pH as displayed in Fig. 5b. In this way, the effect of pH on the drug release could be excluded. The only difference between the two groups lies in that in the tubes containing PRF-JDBM samples, i.e. Group b2, the released $H_2$ from magnesium degradation was speculated to affect the local diffusion process through the coating while $H_2$ produced from PF-JDBM in Group b1 should not interfere with the local drug release from the coating on PR–316 L SS. The effect of $H_2$ evolution on the drug release profiles is revealed in Fig. 5c. The two groups displayed similar release kinetics, i.e., a burst release of about 18% followed by a slower release profile, which seems to be a diffusion-controlled stage. However, during the entire release period, Group b2 released nearly 70% of the total amount of drug while only about 40% in Group b1, indicating that Group b2 exhibited markedly higher drug release rate, about almost twice as compared to Group b1.

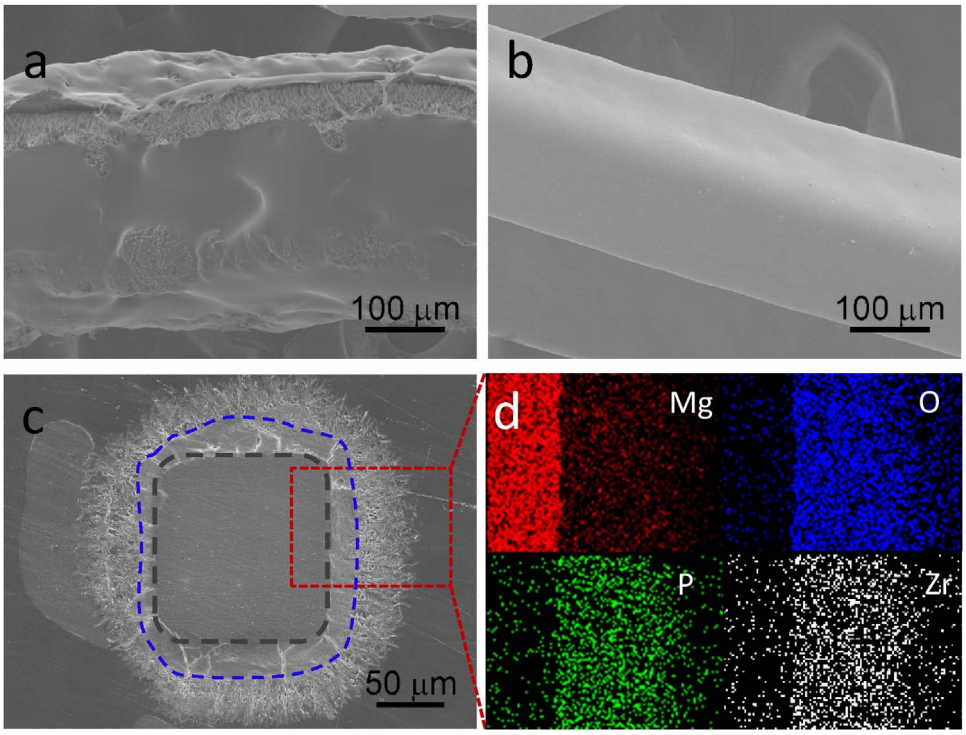


**Fig. 4.** The SEM images of surface morphologies of F-JDBM (a) and 316 L SS DESs (b) at the end of drug release test; and cross-section morphology (c) and local EDS mapping (d) of the F-JDBM DES after dissolving the coating.

### 3.6. The effect of F-JDBM degradation on PLGA hydrolysis

The surface micrographs of PRF-JDBM and 316 L SS samples after immersion in PBST for various time are shown in Fig. 7. The homogeneously distributed tiny island-shaped bulges on the topmost surface before immersion were probably due to the surface segregation of RAPA. After 6 h of release, uniformly distributed pits were observed on the entire surface, most probably owing to the dissolution of RAPA present on the topmost surface of the coating. Bubbles/bulges of different sizes could be attributed to the formation of gas pockets-accumulated $H_2$ generated during the corrosion/degradation of Mg substrates. Micro-cavities started to occur occasionally at day 7 and the formation of submicro- and micro-scale cavities and cracks increased substantially at the end of the third week, with some gas pockets bursting, indicating that the coating started to erode [40]. At the end of the test (58 d), a large portion of the coating surface was damaged and defects/holes of tens of μm size could be observed, which is likely to be caused by the erosion of the PLGA polymeric coating, resulting in the formation of soluble oligomeric fragments and monomer products. On the contrary, the PLGA coating on 316 L SS samples remained smooth and compact with only occasional micro-pores observed, demonstrating much slower hydrolysis of PLGA.

### 3.7. The effect of Mg degradation on RAPA stability

Rapamycin (RAPA) is a natural macrolide immunosuppressant with a structure of a 31-membered macrocycle with 15 stereocenters and multiple functional groups [41], which tends to undergo hydrolysis in acidic or alkaline environment [41,42]. The influence of Mg degradation on the chemical structure of RAPA in PBS containing 30 v/v% IPA was evaluated in a period of 48 h with the use of HPLC. The chromatographic profiles of RAPA in media containing bare Mg, F-JDBM and 316 L SS samples are respectively shown in Fig. 8a–c. The retention time of the RAPA peak was at around 9.0 min. With increasing co-cultivation time, the area of the RAPA peaks decreased whereas the intensity of peaks at around 2.5 min gradually increased, indicating the hydrolysis of RAPA occurred. The percentages of the RAPA remaining in the original chemical structure are displayed in Fig. 8d, calculated based on the corresponding peak area. The peak intensity of remaining RAPA in media containing Mg started to decrease faster than that with 316 L SS after 5 h co-cultivation, suggesting that the degradation of JDBM substrate had deteriorative effect on the hydrolysis of RAPA. With the protection of a $MgF_2$ layer to decelerate Mg substrate degradation, the deterioration was significantly reduced, as only trivial discrepancy ( < 5%) could be observed between the results of F-JDBM and 316 L SS samples even after co-cultivation for 48 h.

Additionally, based on the above results, it is noteworthy that due to the hydrolysis of RAPA, HPLC may not be suitable for measuring the RAPA release profiles in this case. Further study shown in Supplementary Fig. S1 proved that UV–vis spectrophotometry is a more appropriate technique to monitor RAPA release kinetics, as the initial hydrolysis products of RAPA exhibited the same absorption wavelength as RAPA, and thus the data measured by UV–vis spectrophotometry are considered to be more accurate.

### 3.8. In vitro anti-proliferation effect

The short-term inhibitory effect of PRF-JDBM on the proliferation of A7r5 cells were evaluated with direct cell adhesion and proliferation assays, of which the results are shown in Fig. 9. After 1 d of culture, the density of adherent live cells on PRF-JDBM (12 ± 5 cells/mm$^2$) is significantly lower than that on PF-JDBM (24 ± 9 cells/mm$^2$) and the NC group (22 ± 4 cells/mm$^2$). Besides, cell spreading morphology also followed the same trend among these groups, with those on PRF-JDBM appearing abnormal shrunken configuration, a prognostic indicator of poor survival and function. After cultured for 3 days, while the quantities of cells on the other two groups were observed to increase dramatically by almost 3–4 folds, no obvious increase in the live cell density on PRF-JDBM occurred; hence demonstrated a significant inhibitory effect on A7r5 cells proliferation with RAPA loading substrates. The results of in vitro SMC proliferation generally correlate

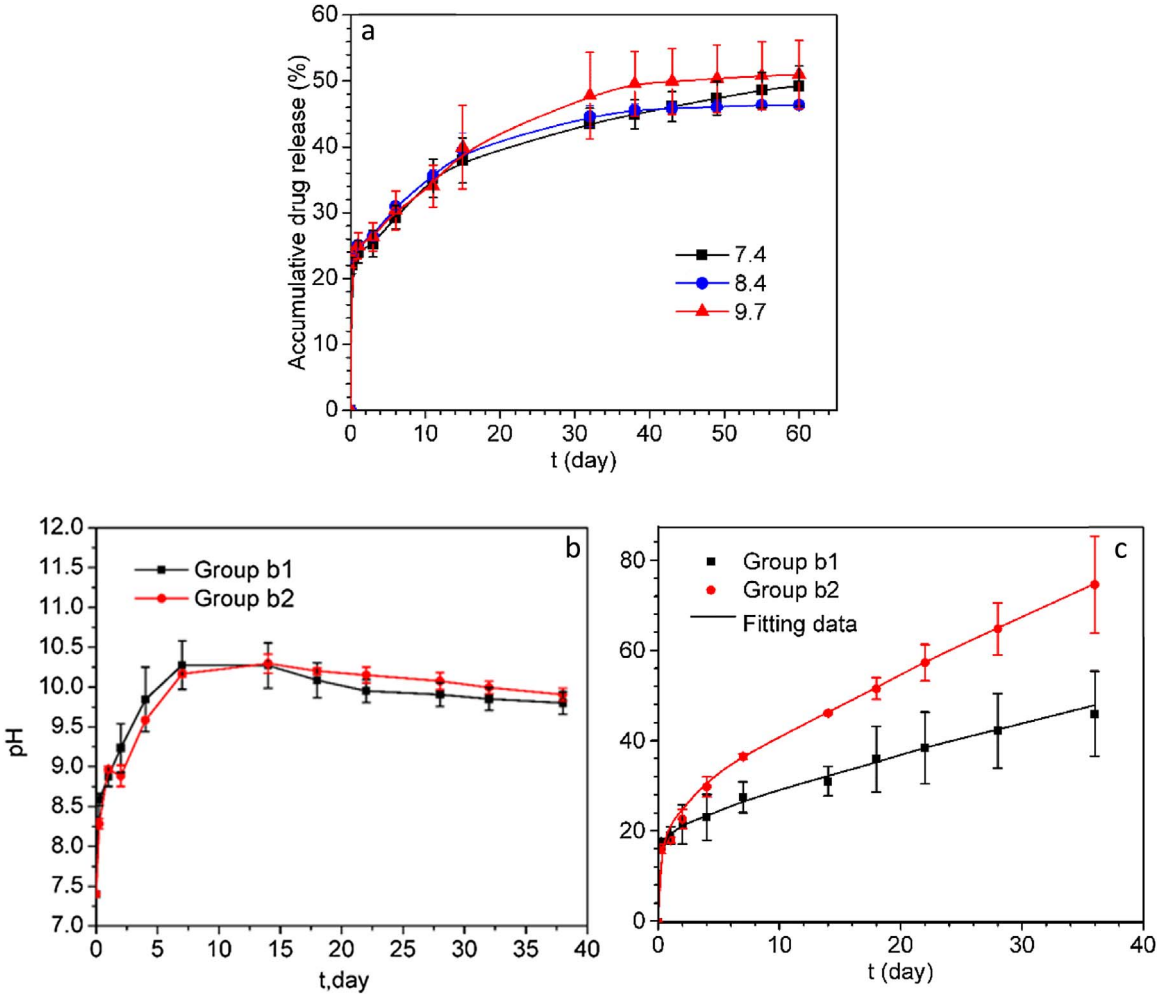


**Fig. 5.** Effect of pH on RAPA release (a); the pH change of Group b1 and Group b2 (b) and effect of $H_2$ evolution generated from magnesium degradation on RAPA release (c) as described in sec.2.6 b. Note that the drug release profiles are fitted using Higuchi model.

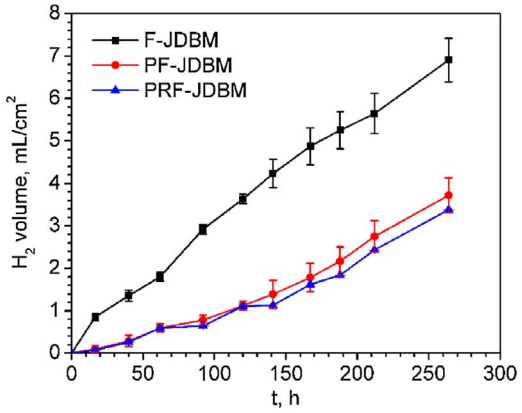


**Fig. 6.** The $H_2$ evolution profiles of F-JDBM, PF-JDBM and PRF-JDBM in c-SBF.

well with the drug release data. The burst release of the drug-loaded coating caused a high initial RAPA concentration, thus greatly inhibiting the cell growth in the first few days.

Generally, the release of the anti-proliferative drug is preferred to last over at least several weeks to suppress SMC proliferation, during which sufficient drug concentration should be delivered [5]. However, during the long-term course, the drug release slowed down dramatically following the initial burst release. Therefore, the long-term inhibition on SMC proliferation worth our concern as well. In this work, in order to eliminate the influence of the initial burst release, cell proliferation on PRF-JDBM and PR–316 L SS, which had already been pre-immersed in DMEM for 10 d prior to cell assays, were also studied and evaluated. Fluorescence micrographs and the statistical analysis of the live cell density in Fig. 10 revealed that a nearly equal number of A7r5 cells were attached onto the PRF-JDBM samples (21 ± 2 cells/$mm^2$) as onto the PR–316 L SS (16 ± 2 cells/$mm^2$) after 1 d of culture, and the cells on both samples did not spread well. Nevertheless, comparing the data of day 1 and day 3, different proliferation rates could be obtained between these two groups of samples. At day 3, the density of A7r5 cells on the PR–316 L SS samples has doubled (34 ± 9 cells/$mm^2$), while on the contrary, no significant difference was observed in terms of cell density on PRF-JDBM samples (22 ± 3 cells/$mm^2$) as compared to day 1, suggesting a more potent long-term inhibitory effect of PRF-JDBM than that of PR–316 L SS.

## 4. Discussion

The inspiring success of BIOSOLVE-I and BIOSOLVE-II trials [10,11] of DREAMS and DREAMS 2G show a bright future of Mg-based DESs as a superior alternative to the conventional permanent implants such as 316 L SS and CoCr alloys. In contrast to the passive metallic substrates, it can be speculated that the magnesium degradation may play a certain role in influencing the drug release kinetics and mechanism, the drug stability as well as the anti-proliferation effect of Mg-based DESs. Nevertheless, so far, little investigation has been found to unravel this issue. Therefore, in this study, we aimed to obtain an in-depth understanding of the in vitro effect of magnesium alloy on the above issues, as

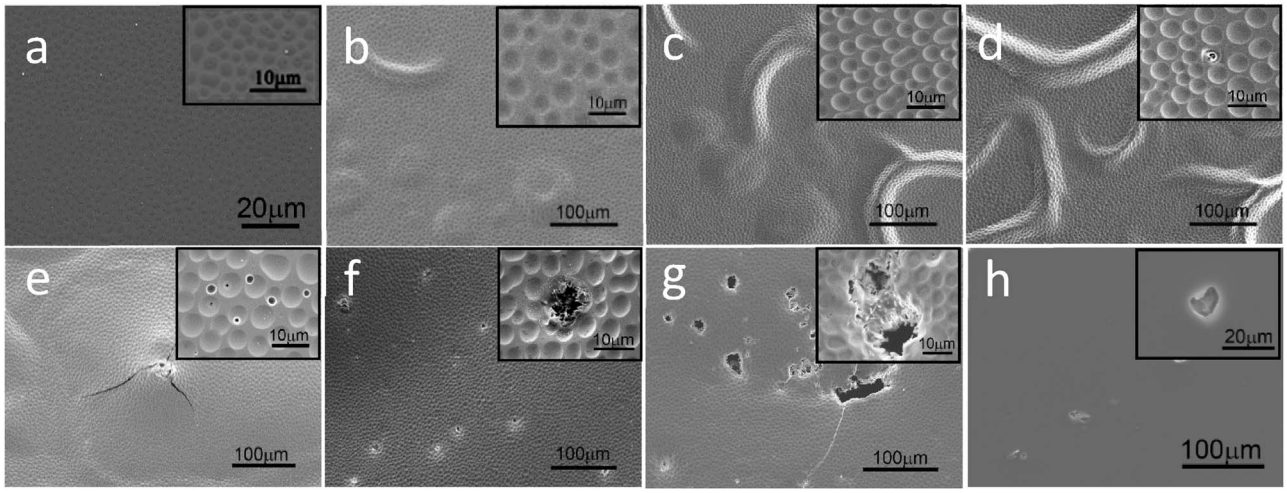


**Fig. 7.** SEM micrographs of the coating surface during immersion test, (a) 0 d, (b)1 d, (c) 4 d, (d) 7 d, (e) 21 d, (f) 37 d and (g) 58 d of F-JDBM samples and (h) 58 d of 316 L SS sample.

well as the detailed mechanisms of influencing factors.

### 4.1. Factors contributing to the enhanced drug release

From the drug release data shown in Fig. 3a, the initial burst release (phase I) observed for all the samples in the first day could be contributed to a certain amount of RAPA accumulated on the topmost surface or drug molecules close to the of polymer coating easy accessible by hydration [43].

Following burst release stage, drug release from PLGA is reported to be mainly controlled by diffusion or by erosion (or degradation) of PLGA polymer [40]. In this work, as shown in Fig. 3a, phase II of the profiles is mainly controlled by diffusion. The diffusion-controlled release profile could be analyzed using a Higuchi model [44]:

$$\frac{M_t}{M_0} = kt^{1/2} \tag{3}$$

where $M_t/M_0$ represents the fraction of the drug released, $t$ is the

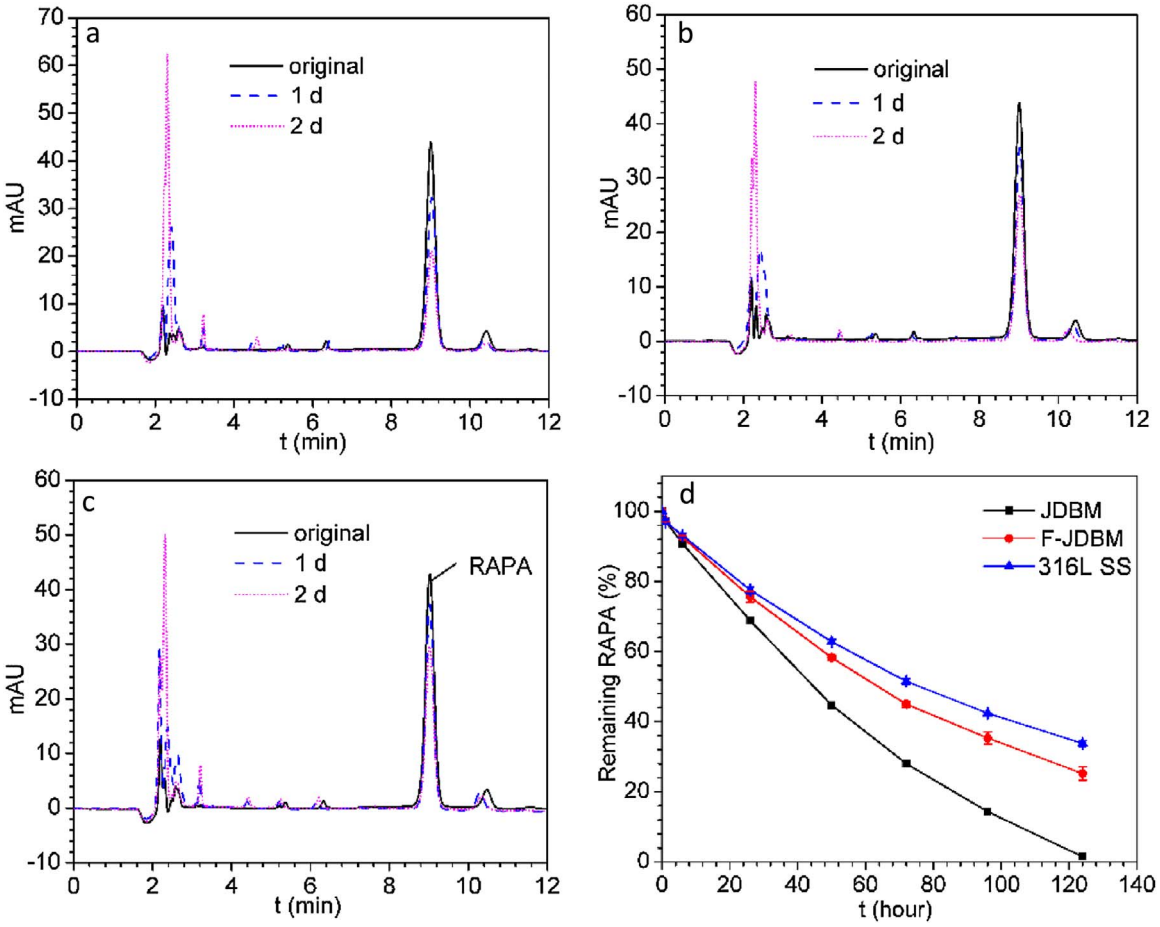


**Fig. 8.** RAPA hydrolysis in media containing naked JDBM (a), F-JDBM (b) and 316 L SS (c) disks and the percentages of the RAPA remaining in the original chemical structure in media respectively containing bare JDBM, F-JDBM and 316 L SS samples vs. immersion time, as calculated from the corresponding peak area of HPLC chromatograms.

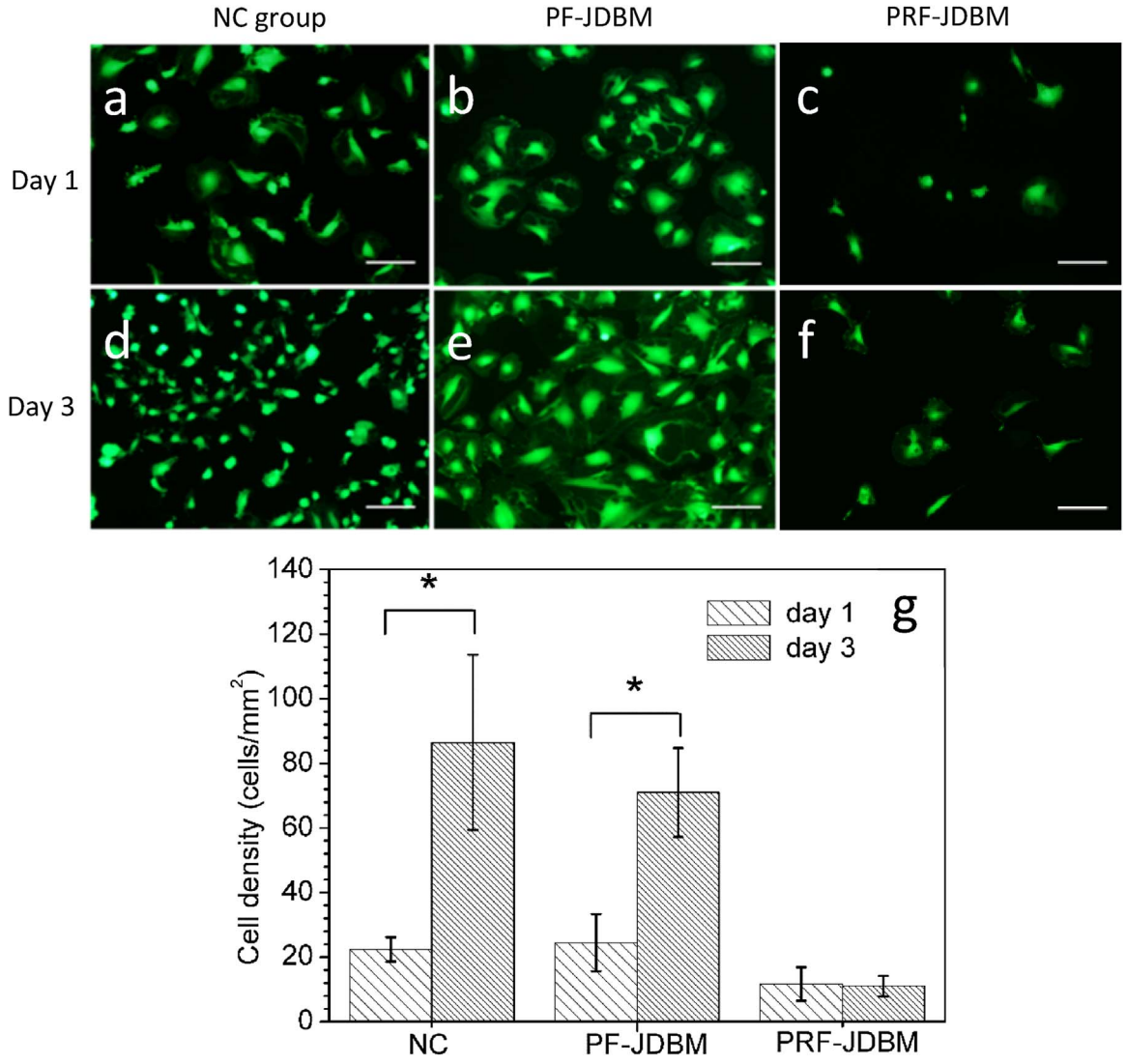


**Fig. 9.** A7r5 cell adhesion and proliferation on (a,d) NC group, (b,e) PF-JDBM, (c,f) PRF-JDBM samples after cultured for (a–c) 1 d and (d-f) 3 d; the scale bars represent 200 μm; and (g) statistical analysis of the adherent live cells on different samples. *$p < 0.05$.

release time and $k$ is a constant characteristic of the system.

The value of the diffusion coefficient, $D$, can be calculated according to the formula [44]:

$$k = 4\left(\frac{D}{\pi l^2}\right)^{1/2} \tag{4}$$

where $l$ is the thickness of the coating. Eq. (4) is valid for release of less than 60% of the initial drug load, which is applied along with Eq. (3) to calculate $D$ value.

Table 3 presents the constant $k$ of phase II fitted using Eq. (3) from the release profiles of both groups of DESs and the diffusion coefficients $D$ obtained from Eqs. (3) and (4). F-JDBM stents exhibited significantly faster drug release ($k$ = 11.2% day$^{-1}$) than PR–316 L SS ($k$ = 1.47% day$^{-1}$). Apparently, the distinctions in terms of drug release rate were mainly attributed to the different diffusion coefficients D, with a value of $2.05 \times 10^{-14}$ cm$^2$/s for 316 L SS DES, and $1.19 \times 10^{-15}$ cm$^2$/s for F-JDBM DES, respectively.

Further studies have been performed to prove the detailed mechanisms at phase II. Based on the results illustrated in Fig. 5, the improvement of drug release was corroborated to be caused by these two possible factors: 1) alkaline environment and 2) $H_2$ release resulting from magnesium degradation. The drug release kinetics profiles shown in Fig. 5a and c, which were designed to explore the respective roles of these two factors, were also fitted and analyzed using a Higuchi model, with the modeling results listed in Table 4.

Apparently, limited influence of pH on the burst release was observed as shown in Fig. 5a. In the pH range of 7.4–9.7, the RAPA release profile was hardly affected which could be attributed to the hydrolysis mechanism of PLGA. Once PLGA directly contacts with aqueous solution, it undergoes hydrolysis, which has been proven to be catalyzed by acid or base. After a while, the hydrolysis of PLGA led to the formation of pores and cracks in the polymer coating and also more intermediate degradation products, mainly oligomers and monomers, which typically have carboxylic groups. The degradation of the polymer is generally assumed to be auto-catalyzed by the carboxylic acid end groups accumulated inside the pores [45–47]. It was found that the pH inside the pores of eroding anhydrides was between 4 and 5, far below that of the bulk medium which was 7.4 [48]. Even lower pH in the eroding polymer was observed for PLA and its copolymers, due to the higher solubility and the low p$K_a$ compared with the poly(anhydride) monomers [49]. Thus, higher pH of bulk solution accelerated the hydrolysis of PLGA in the initial stage, resulting in a pH decrease inside the polymer coating due to the generation of degradation products, meanwhile the penetrated solution with a pH range of 7.4-9.7 could neutralize the acidic degradation products in the microenvironment, and thus the autocatalysis of carboxylic acid end groups on polymer

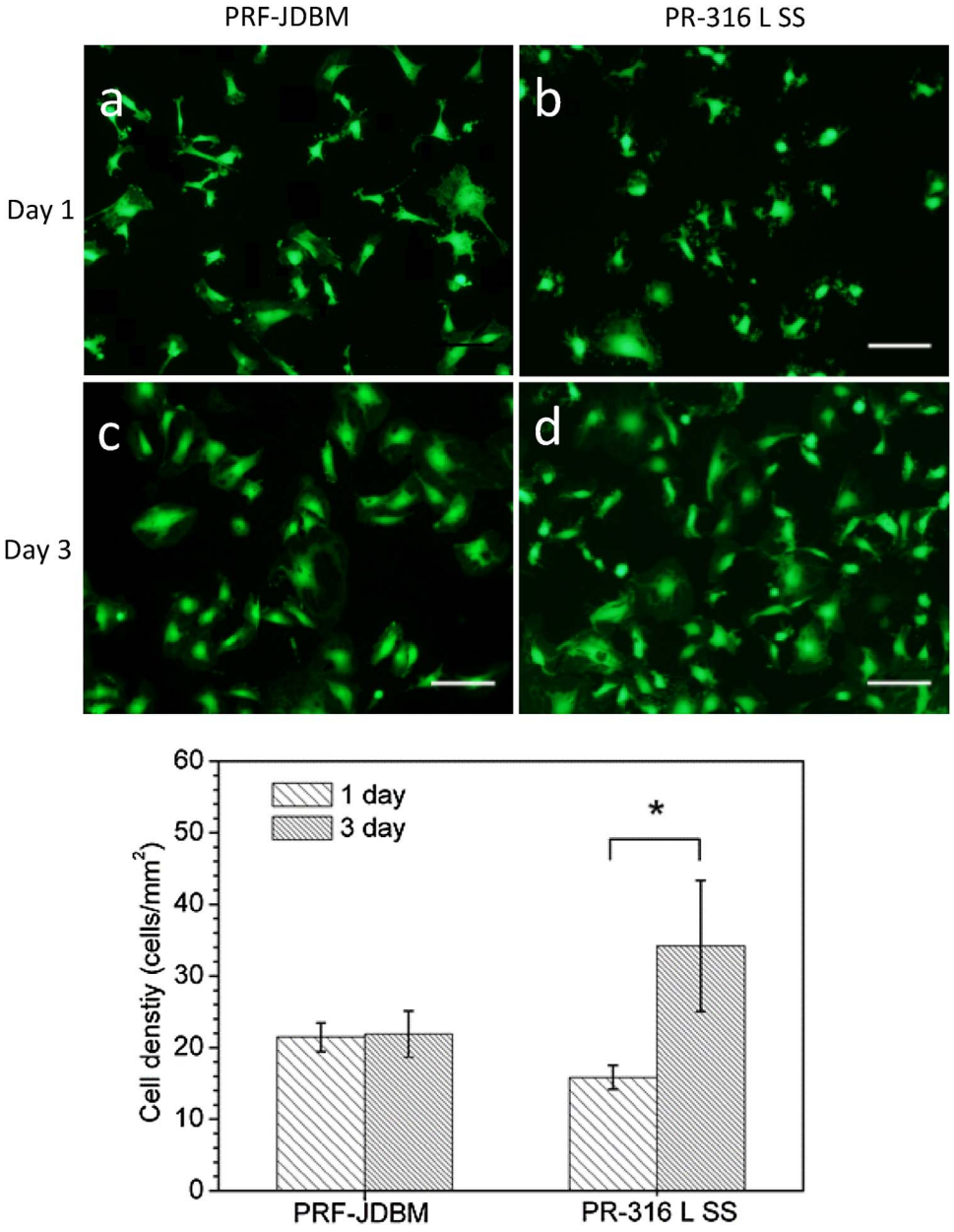


**Fig. 10.** A7r5 cell adhesion and proliferation on (a,c) PRF-JDBM and (b,d) PR–316 L SS samples after cultured for (a,b) 1 d and (c,d) 3 d; the scale bars represent 200 μm; and (e) statistical analysis of the adherent live cells, *p < 0.05. Note that prior to the cell assays, the samples had been immersed in DMEM for 10 days to eliminate the burst drug release.

**Table 3**
Results calculated from the phase II of RAPA release kinetics using Higuchi model.

| Substrate | Period (days) | *k* (%/day) | $R^2$ | D ($cm^2$/s) |
|---|---|---|---|---|
| F-JDBM | 2–33 | 11.2 | 0.992 | $1.19 \times 10^{-15}$ |
| SS | 2–63 | 1.47 | 0.994 | $2.05 \times 10^{-17}$ |

**Table 4**
Calculated results of drug release kinetics affected by pH and $H_2$ evolution using Higuchi model..

| Effect of $H_2$ | Period (days) | *k* (%/day) | $R^2$ | D($cm^2$/s) |
|---|---|---|---|---|
| Group b1 | 2–36 | 5.61 | 0.987 | $2.98 \times 10^{-16}$ |
| Group b2 | 2–36 | 10.37 | 0.991 | $1.02 \times 10^{-15}$ |

chain cleavage might be hindered. An earlier study found the biodegradation rate of PLGA (with LA/GA ratio of 50/50) decreased and reached a plateau in a basic medium (pH 9.24) whereas polymers in the media of pH 5.0 kept degrading [50]. According to these previous findings, it can be inferred that the hydrolysis of PLGA might not be promoted in a weak alkaline environment with pH < 9.7. However, Chu et al. demonstrated that at a higher pH level (pH = 10.09), PLGA showed accelerated degradation than that in slightly acidic or neutral media [51].

On the contrary, it is evident that $H_2$ evolution imposed a prominent role on the drug release kinetics (Fig. 5c), as the *k* value (10.37% $day^{-1}$) of Group b2 almost doubled that (5.61% $day^{-1}$) of Group b1. On one hand, accompanying with the release and diffusion process of the generated $H_2$ through the coating, the diffusion of RAPA could be prompted simultaneously; on the other hand, the formation of $H_2$ pockets, causing micro-scale bulges formed on the Mg substrate as shown in Fig. 7, increased the surface area of polymer coating, which could also facilitate drug diffusion according to Fick's diffusion law.

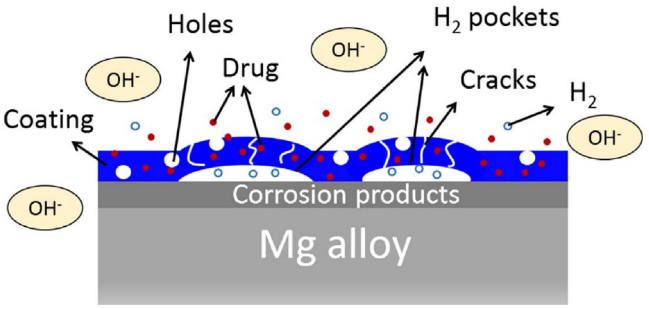


**Fig. 11.** An illustration depicting the possible effects of Mg degradation on drug-loaded PLGA coating that promote drug diffusion.

At phase III of F-JDBM DESs, the linear release profile revealed that this phase was controlled by a combination of diffusion and erosion of PLGA which was found to occur after 37 days of immersion in PBST (Fig. 7f). Many factors can influence PLGA erosion, for instance, overhigh local pH (> 10) and the damaging of $H_2$ when diffusing through the coating are both expected to speed up the degradation of PLGA. Besides, as reported by Chen et al., the products at the interface between the substrate and the coating could react with the coating and also accelerate the degradation of PLGA [52]. Moreover, the flake-like corrosion products in this work caused physical damage to PLGA, which is also considered as an influencing factor.

Based on the above analyses, a mechanism about the effect of magnesium alloy on drug release was proposed as depicted in Fig. 11. At phase II, $H_2$ release greatly enhanced the drug diffusion coefficient throughout the drug release while the influence of pH on the drug release appeared subtle, while at phase III, all factors influencing the PLGA degradation posed an integrated effect on the drug release.

By contrast, as for the passive 316 L SS DESs, as neither $H_2$ nor alkaline environment was generated, accordingly it presented poor drug release profile in terms of both release rate and accumulative release amount, as compared to biodegradable Mg-based DESs.

### 4.2. The effect of magnesium degradation on RAPA stability

The ring cleavage that RAPA can undergo in various conditions could result in ring-opening derivations lacking the macrocycle, which extremely deteriorates the immunosuppressive effect of RAPA [41]. Therefore, apart from RAPA release kinetics, the chemical stability of released RAPA also plays an important part in the anti-restenosis effect. According to the drug stability results shown in Fig. 9, the degradation of Mg alloy has caused certain changes in the chemical structure of RAPA molecule, attributed to the alkaline environment as illustrated in Fig. 3b. Previous studies have demonstrated that the hydrolysis of RAPA is a base or acid catalyzed process [42,53,54], and thus tends to be sensitive to the pH change, which could lead to ring fragmentation and degradation. In contrast to passive substrates, in medium containing bare JDBM, due to the basic environment resulting from magnesium degradation, the hydrolysis of RAPA could be elevated, and a significantly smaller portion of RAPA (~44%) maintained the original chemical structure as compared to 316 L SS (~63%). While for F-JDBM, thanks to the protective $MgF_2$ layer which mitigated magnesium corrosion, its adverse influence on the chemical stability of RAPA was largely alleviated, presenting a similar stability (~58%) feature compared to 316 L SS (Fig. 9). According to the above analysis, proper control of magnesium degradation is imperative, e.g. with additional protective coating, thus reducing the overhigh pH and preventing from the disruption of the RAPA structure, and consequently would be advantageous to suppressing the proliferation of SMCs.

### 4.3. Short- and long-term anti-proliferative effect on SMCs

Vascular smooth muscle cell is an important cell component of neointimal hyperplasia, which has been reported to play a pivotal role in the development and progression of in-stent restenosis following vascular stent implantation [5,55,56]. Apoptosis of vascular smooth muscle cells and inhibition of SMC proliferation is believed to effectively alleviate neointimal hyperplasia and in turn reduce restenosis, which may provide a solution to treat late restenosis.

In our study, corresponding to the drug release measurements, the anti-proliferation effectiveness of RAPA-loaded F-JDBM samples (PRF-JDBM) on SMCs was also examined in vitro. The burst release of the drug accumulated at the topmost surface of the PLGA coating led to a high RAPA concentration in cell culture medium initially and therefore significantly inhibited adhesion and proliferation of smooth muscle cells on PRF-JDBM samples in short-term test, as shown in Fig. 9. Moreover, to investigate the long-term anti-proliferation, cells cultured on PRF-JDBM and PR–316 L SS samples which had been pre-immersed for 10 days in DMEM to eliminate the initial burst release showed distinct adhesion and proliferation behaviours, of which the results correlated well with the long-term drug release profile. The drug-loaded F-JDBM samples exhibited more significant inhibition on the proliferation of SMCs. Correspondingly, from the drug release profile shown in Fig. 3a, it is obvious that from day 10 to day 13, the drug release rate of PRF-JDBM is higher than that of PR–316 L SS, thus displaying superior long-term inhibition of cell proliferation. Based on these in vitro investigations, it could be inferred that the enhanced drug release induced by the degradation of Mg substrate is likely to pose positive influence on the in vivo effectiveness in inhibiting intimal hyperplasia and in-stent restenosis, thus it is worth more concerns on this issue.

It should be noted that the optimal drug release period of DESs should be limited in 1–2 months, as the prolonged drug release is considered to account for delayed re-endothelialization [57]. Another concern is often paid to the local drug concentration, as SMC proliferation could be effectively inhibited only if the drug concentration is beyond a threshhold value [58]. Therefore, a sufficiently high drug concentration within a predictable time period is essential for achieving favorable clinical efficacy of DES treatment. For passive materials, PLGA with higher erosion rate such as PLGA (50/50) of low Mw can be used as the drug-carrier to obtain sufficient local released drug concentration to effectively depress the SMC proliferation. However, in the case of Mg-based DESs, the coating is designed not only to be used as a drug carrier, but also as a barrier layer to suppress Mg corrosion. Rapid erosion of coatings is supposed to lead to diminished protection for Mg-based substrates. From this aspect, PLGA of a higher LA content and high Mw, which is likely to appear slower erosion, is more appropriate to be applied as the drug-carrier in magnesium-based DES systems. Therefore, accelerated drug release from this type of polymer coating with slower degradation rate is beneficial to maintaining the SMC inhibition effect in a relatively long period.

## 5. Conclusion

The drug release kinetics of biodegradable RAPA loaded Mg-Nd-Zn-Zr alloy based DESs were studied comprehensively in a phosphate buffer system in comparison with passive 316L SS DESs, as well as their distinct anti-proliferative effects on the smooth muscle cells. The following conclusions could be obtained from this systematic investigation:

1. The degradation of magnesium alloy substrates greatly accelerated and improved the in vitro drug release kinetics.
2. The enhanced in vitro drug release kinetics was distinguished to be mainly caused by hydrogen evolution and corrosion product produced during the corrosion of the Mg-based substrate through promoting RAPA diffusion, while weakly alkaline pH barely affected

the RAPA release.
3. The RAPA-loaded magnesium alloy samples exhibited more pronounced long-term inhibition on the proliferation of SMCs as compared with drug-loaded passive substrate (316 L SS).

However, it should be noted that this study was mainly carried out in phosphate buffered saline, whose composition greatly differs from a true biofluid system, thus there is a limitation to relate the findings here directly to in vivo conditions which are worth further investigation.

## Author contributions

G. Yuan and J. Pei designed the study. Y. Shi performed the study and drafted the manuscript. Z. Li and L. Zhang helped prepare the samples. S. Gu helped do cell experiments. J. Pei, K. Park, B. Lee, Y. Yun, J. Zhang, and G. Yuan revised the manuscript. All authors reviewed the manuscript.

## Notes

The authors declare no competing financial interest.

## Acknowledgements

This work was financially supported by the National Natural Scientific Foundation of China (No.51571143, No.51501115), the Science and Technology Commission of Shanghai Municipality (No. 14DZ1940800, No. 17XD1402100) and the National Key Research and Development Program of China (2016 YFC1102400).

## Appendix A. Supplementary data

Supplementary data associated with this article can be found, in the online version, at http://dx.doi.org/10.1016/j.corsci.2017.04.016.

## References

[1] I. Akin, H. Schneider, H. Ince, S. Kische, T. Rehders, T. Chatterjee, C. Nienaber, Second-and third-generation drug-eluting coronary stents, Herz 36 (2011) 190–197.
[2] G.J. Laarman, M.J. Suttorp, M.T. Dirksen, L. van Heerebeek, F. Kiemeneij, T. Slagboom, L.R. van der Wieken, J.G. Tijssen, B.J. Rensing, M. Patterson, Paclitaxel-eluting versus uncoated stents in primary percutaneous coronary intervention, N. Engl. J. Med. 355 (2006) 1105–1113.
[3] J.W. Moses, M.B. Leon, J.J. Popma, P.J. Fitzgerald, D.R. Holmes, C. O'Shaughnessy, R.P. Caputo, D.J. Kereiakes, D.O. Williams, P.S. Teirstein, Sirolimus-eluting stents versus standard stents in patients with stenosis in a native coronary artery, N. Engl. J. Med. 349 (2003) 1315–1323.
[4] R. BEYAR, Novel approaches to reduce restenosis, Ann. N. Y. Acad. Sci. 1015 (2004) 367–378.
[5] T.C. Woods, A.R. Marks, Drug-eluting stents, Annu. Rev. Med. 55 (2004) 169–178.
[6] P. Erne, M. Schier, T.J. Resink, The road to bioabsorbable stents: reaching clinical reality? Cardiovasc. Intervent. Radiol. 29 (2005) 11–16.
[7] D. Schranz, P. Zartner, I. Michel-Behnke, H. Akinturk, Bioabsorbable metal stents for percutaneous treatment of critical recoarctation of the aorta in a newborn, Catheter. Cardiovasc. Interv. 67 (2006) 671–673.
[8] G. Song, Control of biodegradation of biocompatable magnesium alloys, Corros. Sci. 49 (2007) 1696–1701.
[9] R. Erbel, C. Di Mario, J. Bartunek, J. Bonnier, B. de Bruyne, F.R. Eberli, P. Erne, M. Haude, B. Heublein, M. Horrigan, C. Ilsley, D. Böse, J. Koolen, T.F. Lüscher, N. Weissman, R. Waksman, Temporary scaffolding of coronary arteries with bioabsorbable magnesium stents: a prospective non-randomised multicentre trial, Lancet 369 (2007) 1869–1875.
[10] M. Haude, R. Erbel, P. Erne, S. Verheye, H. Degen, D. Böse, P. Vermeersch, I. Wijnbergen, N. Weissman, F. Prati, R. Waksman, J. Koolen, Safety and performance of the drug-eluting absorbable metal scaffold (DREAMS) in patients with de-novo coronary lesions: 12 month results of the prospective, multicentre, first-in-man BIOSOLVE-I trial, Lancet 381 (2013) 836–844.
[11] M. Haude, H. Ince, A. Abizaid, R. Toelg, P.A. Lemos, C. von Birgelen, E.H. Christiansen, W. Wijns, F.-J. Neumann, C. Kaiser, E. Eeckhout, S.T. Lim, J. Escaned, H.M. Garcia-Garcia, R. Waksman, Safety and performance of the second-generation drug-eluting absorbable metal scaffold in patients with de-novo coronary artery lesions (BIOSOLVE-II): 6 month results of a prospective, multicentre, non-randomised, first-in-man trial, Lancet 387 (2016) 31–39.
[12] B. Heublein, R. Rohde, V. Kaese, M. Niemeyer, W. Hartung, A. Haverich, Biocorrosion of magnesium alloys: a new principle in cardiovascular implant technology? Heart 89 (2003) 651–656.
[13] R. Waksman, R. Erbel, C. Di Mario, J. Bartunek, B. de Bruyne, F.R. Eberli, P. Erne, M. Haude, M. Horrigan, C. Ilsley, D. Böse, H. Bonnier, J. Koolen, T.F. Lüscher, N.J. Weissman, Early- and long-term intravascular ultrasound and angiographic findings after bioabsorbable magnesium stent implantation in human Coronary arteries, JACC Cardiovasc. Interv. 2 (2009) 312–320.
[14] R. Waksman, R. Pakala, P.K. Kuchulakanti, R. Baffour, D. Hellinga, R. Seabron, F.O. Tio, E. Wittchow, S. Hartwig, C. Harder, R. Rohde, B. Heublein, A. Andreae, K.-H. Waldmann, A. Haverich, Safety and efficacy of bioabsorbable magnesium alloy stents in porcine coronary arteries, Catheter. Cardiovasc. Interv. 68 (2006) 607–617.
[15] E. Wittchow, N. Adden, J. Riedmueller, C. Savard, R. Waksman, M. Braune, Bioresorbable drug-eluting magnesium-alloy scaffold: design and feasibility in a porcine coronary model, EuroIntervention 8 (2013) 1441–1450.
[16] H. Li, H. Zhong, K. Xu, K. Yang, J. Liu, B. Zhang, F. Zheng, Y. Xia, L. Tan, D. Hong, Enhanced efficacy of sirolimus-eluting bioabsorbable magnesium alloy stents in the prevention of restenosis, J. Endovasc. Ther. 18 (2011) 407–415.
[17] P. Zartner, R. Cesnjevar, H. Singer, M. Weyand, First successful implantation of a biodegradable metal stent into the left pulmonary artery of a preterm baby, Catheter. Cardiovasc. Interv. 66 (2005) 590–594.
[18] M. Haude, H. Ince, A. Abizaid, R. Toelg, P.A. Lemos, C. von Birgelen, E.H. Christiansen, W. Wijns, F.-J. Neumann, C. Kaiser, safety and performance of the second-generation drug-eluting absorbable metal scaffold in patients with de novo coronary lesions: 12-month clinical results and angiographic findings of the BIOSOLVE-II first-in-man trial, Eur. Heart J. (2016) (ehw196.).
[19] G. Acharya, K. Park, Mechanisms of controlled drug release from drug-eluting stents, Adv. Drug Del. Rev. 58 (2006) 387–401.
[20] R.-C. Zeng, Y. Hu, S.-K. Guan, H.-Z. Cui, E.-H. Han, Corrosion of magnesium alloy AZ31: The influence of bicarbonate, sulphate, hydrogen phosphate and dihydrogen phosphate ions in saline solution, Corros. Sci. 86 (2014) 171–182.
[21] L. Mao, G. Yuan, J. Niu, Y. Zong, W. Ding, In vitro degradation behavior and biocompatibility of Mg–Nd–Zn–Zr alloy by hydrofluoric acid treatment, Mater. Sci. Eng. C 33 (2013) 242–250.
[22] Z. Li, X. Gu, S. Lou, Y. Zheng, The development of binary Mg–Ca alloys for use as biodegradable materials within bone, Biomaterials 29 (2008) 1329–1344.
[23] N.I. Zainal Abidin, B. Rolfe, H. Owen, J. Malisano, D. Martin, J. Hofstetter, P.J. Uggowitzer, A. Atrens, The in vivo and in vitro corrosion of high-purity magnesium and magnesium alloys WZ21 and AZ91, Corros. Sci. 75 (2013) 354–366.
[24] J. Ma, N. Zhao, D. Zhu, Biphasic responses of human vascular smooth muscle cells to magnesium ion, J. Biomed. Mater. Res. A 104 (2016) 347–356.
[25] A. Samaniego, I. Llorente, S. Feliu Jr., Combined effect of composition and surface condition on corrosion behaviour of magnesium alloys AZ31 and AZ61, Corros. Sci. 68 (2013) 66–71.
[26] I. Ročňáková, E.B. Montufar, M. Horynová, T. Zikmund, K. Novotný, L. Klakurková, L. Čelko, G.-L. Song, J. Kaiser, Assessment of localized corrosion under simulated physiological conditions of magnesium samples with heterogeneous microstructure: value of X-ray computed micro-tomography platform, Corros. Sci. 104 (2016) 187–196.
[27] L. Mao, L. Shen, J. Niu, J. Zhang, W. Ding, Y. Wu, R. Fan, G. Yuan, Nanophasic biodegradation enhances the durability and biocompatibility of magnesium alloys for the next-generation vascular stents, Nanoscale 5 (2013) 9517–9522.
[28] X. Zhang, G. Yuan, L. Mao, J. Niu, W. Ding, Biocorrosion properties of as-extruded Mg–Nd–Zn–Zr alloy compared with commercial AZ31 and WE43 alloys, Mater. Lett. 66 (2012) 209–211.
[29] J. Zhang, N. Kong, J. Niu, Y. Shi, H. Li, Y. Zhou, G. Yuan, Influence of fluoride treatment on surface properties, biodegradation and cytocompatibility of Mg-Nd-Zn-Zr alloy, J. Mater. Sci. Mater. Med. 25 (2013) 791–799.
[30] H.K. Makadia, S.J. Siegel, Poly lactic-co-glycolic acid (PLGA) as biodegradable controlled drug delivery carrier, Polymers 3 (2011) 1377–1397.
[31] C.-H. Lee, S.-H. Chang, Y.-H. Lin, S.-J. Liu, C.-J. Wang, M.-Y. Hsu, K.-C. Hung, Y.-H. Yeh, W.-J. Chen, I.C. Hsieh, M.-S. Wen, Acceleration of re-endothelialization and inhibition of neointimal formation using hybrid biodegradable nanofibrous rosuvastatin-loaded stents, Biomaterials 35 (2014) 4417–4427.
[32] A. Finkelstein, D. McClean, S. Kar, K. Takizawa, K. Varghese, N. Baek, K. Park, M.C. Fishbein, R. Makkar, F. Litvack, Local drug delivery via a coronary stent with programmable release pharmacokinetics, Circulation 107 (2003) 777–784.
[33] T. Xi, R. Gao, B. Xu, L. Chen, T. Luo, J. Liu, Y. Wei, S. Zhong, In vitro and in vivo changes to PLGA/sirolimus coating on drug eluting stents, Biomaterials 31 (2010) 5151–5158.
[34] H. Hara, M. Nakamura, J.C. Palmaz, R.S. Schwartz, Role of stent design and coatings on restenosis and thrombosis, Adv. Drug Del. Rev. 58 (2006) 377–386.
[35] M.L. Forrest, C.-Y. Won, A.W. Malick, G.S. Kwon, In vitro release of the mTOR inhibitor rapamycin from poly(ethylene glycol)-b-poly(ε-caprolactone) micelles, J. Control. Release 110 (2006) 370–377.
[36] S. Chen, L. Tan, Y. Teng, B. Zhang, K. Yang, Study of drug-eluting coating on metal coronary stent, Mater. Sci. Eng. C 33 (2013) 1476–1480.
[37] M. Liu, P. Schmutz, P.J. Uggowitzer, G. Song, A. Atrens, The influence of yttrium (Y) on the corrosion of Mg–Y binary alloys, Corros. Sci. 52 (2010) 3687–3701.
[38] C.P. Naseerali, P.R. Hari, K. Sreenivasan, The release kinetics of drug eluting stents containing sirolimus as coated drug: role of release media, J. Chromatogr. B 878 (2010) 709–712.
[39] S. Mandel, A.C. Tas, Brushite ($CaHPO_4{\cdot}2H_2O$) to octacalcium phosphate ($Ca_8(HPO_4)_2(PO_4)_4{\cdot}5H_2O$) transformation in DMEM solutions at 36.5 °C, Mater. Sci.

Eng. C 30 (2010) 245–254.
[40] X. Wang, S.S. Venkatraman, F.Y.C. Boey, J.S.C. Loo, L.P. Tan, Controlled release of sirolimus from a multilayered PLGA stent matrix, Biomaterials 27 (2006) 5588–5595.
[41] Y.V. Il'ichev, L. Alquier, C.A. Maryanoff, Degradation of rapamycin and its ring-opened isomer: role of base catalysis, Arkivoc 12 (2007) 110–131.
[42] F.C. Nelson, S.J. Stachel, C.P. Eng, S.N. Sehgal, Manipulation of the C(22)-C(27) region of rapamycin: stability issues and biological implications, Biorg. Med. Chem. Lett. 9 (1999) 295–300.
[43] J. Wang, B.M. Wang, S.P. Schwendeman, Characterization of the initial burst release of a model peptide from poly (D, L-lactide-co-glycolide) microspheres, J. Control. Release 82 (2002) 289–307.
[44] F. Alexis, S.S. Venkatraman, S.K. Rath, F. Boey, In vitro study of release mechanisms of paclitaxel and rapamycin from drug-incorporated biodegradable stent matrices, J. Control. Release 98 (2004) 67–74.
[45] L. Lu, C.A. Garcia, A.G. Mikos, In vitro degradation of thin poly (DL-lactic-co-glycolic acid) films, J. Biomed. Mater. Res. 46 (1999) 236–244.
[46] S.S. Shah, Y. Cha, C.G. Pitt, Poly (glycolic acid-co-dl-lactic acid): diffusion or degradation controlled drug delivery? J. Control. Release 18 (1992) 261–270.
[47] M. Vert, S. Li, H. Garreau, More about the degradation of LA/GA-derived matrices in aqueous media, J. Control. Release 16 (1991) 15–26.
[48] A. Göpferich, R. Langer, The influence of microstructure and monomer properties on the erosion mechanism of a class of polyanhydrides, J. Polym. Sci. A: Polym. Chem. 31 (1993) 2445–2458.
[49] A. Göpferich, Mechanisms of polymer degradation and erosion, Biomaterials 17 (1996) 103–114.
[50] X.S. Wu, N. Wang, Synthesis, characterization, biodegradation, and drug delivery application of biodegradable lactic/glycolic acid polymers Part II: biodegradation, J. Biomater. Sci. Polym. Ed. 12 (2001) 21–34.
[51] C.C. Chu, A comparison of the effect of pH on the biodegradation of two synthetic absorbable sutures, Ann. Surg. 195 (1982) 55–59.
[52] Y. Chen, Y. Song, S. Zhang, J. Li, C. Zhao, X. Zhang, Interaction between a high purity magnesium surface and PCL and PLA coatings during dynamic degradation, Biomed. Mater. 6 (2011) 025005.
[53] R.J. Steffan, R.M. Kearney, D.C. Hu, A.A. Failli, J.S. Skotnicki, R.A. Schiksnis, J.F. Mattes, K.W. Chan, C.E. Caufield, Base catalyzed degradations of rapamycin, Tetrahedron Lett. 34 (1993) 3699–3702.
[54] J.I. Luengo, A.L. Konialian, D.A. Holt, Studies on the chemistry of rapamycin: novel transformations under lewis-acid catalysis, Tetrahedron Lett. 34 (1993) 991–994.
[55] R. Fattori, T. Piva, Drug-eluting stents in vascular intervention, Lancet 361 (2003) 247–249.
[56] M. Poon, S.O. Marx, R. Gallo, J.J. Badimon, M.B. Taubman, A.R. Marks, Rapamycin inhibits vascular smooth muscle cell migration, J. Clin. Invest. 98 (1996) 2277.
[57] M. Joner, G. Nakazawa, A.V. Finn, S.C. Quee, L. Coleman, E. Acampado, P.S. Wilson, K. Skorija, Q. Cheng, X. Xu, Endothelial cell recovery between comparator polymer-based drug-eluting stents, J. Am. Coll. Cardiol. 52 (2008) 333–342.
[58] P. Burton, M. Yacoub, P. Barton, Rapamycin (sirolimus) inhibits heart cell growth in vitro, Pediatr. Cardiol. 19 (1998) 468–470.